Comparison of Harris Detector and Ridge Bifurcation Points in the Process of Fingerprint Registration using Supervised Contactless Biometric System

Tahirou DJARA, Marc Kokou ASSOGBA, Amine NAÏT-ALI, Antoine VIANOU

Abstract— Most of the matching or verification phases of the contact based fingerprint verification systems utilize minutiae to find the matched pairs from the input and template fingerprints. Unfortunately, due to some non-linear distortions, like excessive pressure and twisting of fingers during enrollment, this process can cause the minutiae features to be distorted from the original. Contact-based fingerprint systems have some drawbacks due to skin elasticity, inconsistent finger placement, contact pressure, small sensing area, environment conditions and sensor noise... In this paper, we present two fingerprint registration algorithms based on Harris Detector and Minutiae matching for a Contactless Biometric system approach. The performances of the algorithms are evaluated using statistical mean and variance. Based on the above measures, the most efficient registration algorithm is pointed out.

Keyword—Contactless Biometrics, Fingerprint, Harris Detector, Ridge Bifurcation, Registration, Variance, Mean.

I. INTRODUCTION

Biometric authentication has received extensive attention over the past decade with increasing demands in automated personal identification as fingerprints are assumed to be unique across individuals, and fingers of the same individual. [1]. Fingerprint systems available today are in general contact-based for which acquisition of fingerprint images is performed by pressing or rolling fingers on a glass or plastic surface. However, these systems have some drawbacks due to skin elasticity, inconsistent finger placement, contact pressure, small sensing area, environment conditions and sensor noise. Additionally, problems like contagious diseases spreading make the use of contact-based scanners not very safe. In order to solve the innate problems of contact-based sensors, various type of contactless sensors are being developed. Also, a large variety of algorithms have been proposed in order to achieve better authentication performance.

Fingerprint registration is a critical step when dealing with fingerprint matching. The registration is a classic problem in computer vision that occurs in many tasks of analysis and image processing. Although a wide variety of registration algorithms have been proposed, the precise registration of fingerprints remains an unresolved problem [2]. In an earlier work, C. Harris and M. Stephens have shown that corners and edges can be directly matchable when detected by using an appropriate local auto-correlation response function. Other works have improved the Harris detector [3].

In this paper, we present two fingerprint registration algorithms based on Harris feature points and bifurcation points matching. The first algorithm uses bifurcation points and the second one uses the Harris feature points. For both, matching is checked by computing Zernike moment vectors on a window of size RxR centered at each point. Comparison of correlation coefficients between Zernike moment descriptors is used to define the corresponding points. The estimation of parameters of the existing deformation between the images is performed using RANSAC algorithm (Random SAmple Consensus) that remove false correspondences.

The used images are obtained from a supervised contactless image acquisition system. Figure 1 shows a contactless acquisition fingerprint image.

Figure 1: Contactless Fingerprint image

Tahirou DJARA, Laboratoire d'Electrotechnique, de Télécommunications et d'Informatique Appliquée (LETIA), Ecole Polytechnique d'Abomey-Calavi (EPAC). Université d'Abomey-Calavi Laboratoire Images, Signaux et Systèmes Intelligents Université Paris-Est Créteil 61, avenue du Général de Gaulle 94010,Créteil France.

Marc Kokou ASSOGBA, Laboratoire d'Electrotechnique, de Télécommunications et d'Informatique Appliquée (LETIA), Ecole Polytechnique d'Abomey-Calavi (EPAC). Université d'Abomey-Calavi .

Amine NAÏT-ALI, Laboratoire Images, Signaux et Systèmes Intelligents Université Paris-Est Créteil 61, avenue du Général de Gaulle 94010,Créteil .

Antoine VIANOU, Laboratoire d'Electrotechnique, de Télécommunications et d'Informatique Appliquée (LETIA) Ecole Polytechnique d'Abomey-Calavi (EPAC). Université d' Abomey-Calavi .

Retrieval Number: F0808052613/13©BEIESP
Journal Website: www.ijitee.org

197

Published By:
Blue Eyes Intelligence Engineering
and Sciences Publication (BEIESP)
© Copyright: All rights reserved.

The paper is structured as follows. The experimental setup is presented in section 2. The principle of the two algorithms is presented in section 3. Section 4 contains the comparative study of the experimental results. Section 5 concludes our work.

II. EXPERIMENTAL SETUP

In the literature, there are few studies focused on contactless systems [4, 5]. Most systems require the placement of the finger on predisposed guides in order to simplify the image acquisition step [4, 6].

A. Image Acquisition

We have developed a platform for the acquisition of images (Figure 2). The contactless fingerprint acquisition system that we have developed consists of this platform to visualize the sharpness of the images before capture, a webcam for taking digital photo, and lighting equipment.

The user is prompted to place the reverse of his finger on a desk. The Palm of the user is faced with the webcam. We proceed to the capture of fingerprint. In order to limit travel, a rectangular area is defined on the interface of the webcam which will contain the finger before capture.
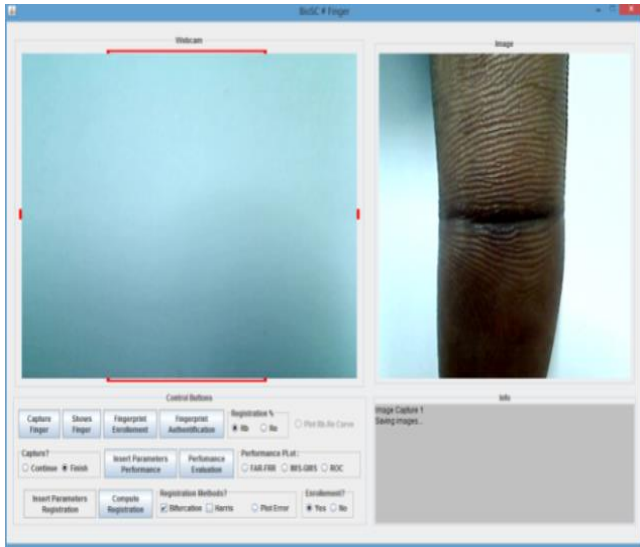

Figure 2: Capture interface

B. Pre-processing phase

Pre-processing plays a significant role in improving image contrast. We have used histogram equalization for image enhancement

III. PRINCIPLE OF THE ALGORITHMS

The registration includes five steps for the first algorithm and four steps for the second. The details are as follows:
1. Image segmentation is performed in order to extract ridges and valleys. The resulting image is skeletonized in order to reduce the thickness of ridges. The skeletonized image is used for detection of ridge bifurcation points,
2. A set of Harris feature points to be matched from the reference image and the input image is selected,
3. Zernike moments are computed as feature descriptors,
4. Definition of a similarity measure to establish a correspondence between the detected corresponding points from the two images,
5. Finally, once the sets of the corresponding points are obtained, the parameters that modeling the best deformation

between these sets are estimated. The deformation is then extended to all pixels from the input image.

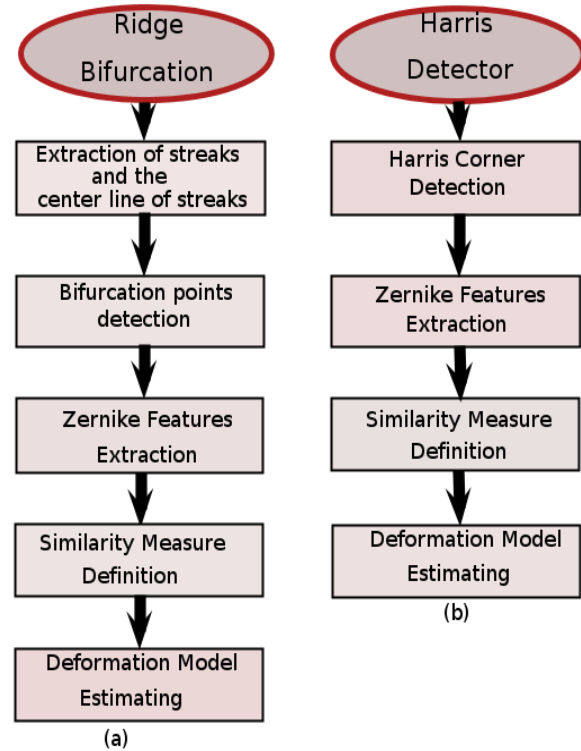Figure 3 shows a flowchart of two algorithms.

Figure 3: A flowchart of two algorithms: (a) Ridge Bifurcation (b) Harris Detector

A. Ridge bifurcation points detection

In order to characterize the fingerprint images, a photometric adaptive threshold method has been developed and presented in [7]. Two thresholds are defined i.e. S_s and S_h corresponding to the mean of a square framework and the mean of a hexagonal framework. A pixel $P(x, y)$ is deleted or not by comparing its value with S_s and S_h. The photometric segmentation is followed by a morphometric segmentation. The image from the segmentation is skeletonized in order to get bifurcation points. The first step in a process of automatic image registration of fingerprints involves the automatic selection a set of potential control points from two images to realign F_t and F_{t+d}. The performance at this stage of selection of control points is important because it depicts the quality of registration.
Bifurcations points are extracted by classic minutiae detection algorithm.

B. Harris feature points detection

The problem addressed by Harris and Stephens [8] is that of using computer vision to understand the unconstrained 3D world, in which the viewed scenes will in general contain too wide a diversity of objects for top-down recognition techniques to work. Their solution is to attempt to detect both edges and corners in images. They referred to the Moravec corner detector [9, 10] which suffers from a number of problems they listed with appropriate corrective measures. Moravec's corner detector considers a local window in the image, and determines the average changes of image intensity that result from shifting the window by a small amount in various directions. The basic idea of the Harris and Stephens detector is to use

the autocorrelation function to determine the positions where the signal changes in two directions simultaneously. Taking into account the first derivatives on a window σ, a matrix M related to the autocorrelation function is calculated:

$$M = e^{-\frac{x^2+y^2}{2\sigma^2}} \times \begin{bmatrix} I_x^2 & I_x I_y \\ I_x I_y & I_y^2 \end{bmatrix} \qquad (1)$$

($\times$) stands for the ordinary multiplication.

where $I_x = \frac{\partial I}{\partial x}$, $I_y = \frac{\partial I}{\partial y}$ and $G(\sigma) = e^{-\frac{x^2+y^2}{2\sigma^2}}$ represents a Gaussian smoothing. The eigenvalues of this matrix are the principal curvatures of the autocorrelation function. Two large enough values indicate the presence of a point of interest. The use of curvature is more accurate than the use of the minimum value as suggested by Moravec. However, to avoid an explicit calculation of the eigenvalues, Harris uses a measure based on the determinant and trace of the matrix. The corners are then extracted from the following operator:

$$Det(M) - k \times Trace^2(M) \qquad (2)$$

where k is a parameter for combining information from outline given by the trace of M with the information of angularity given by the determinant of M. Figure 4 shows an example of landmarks detection.
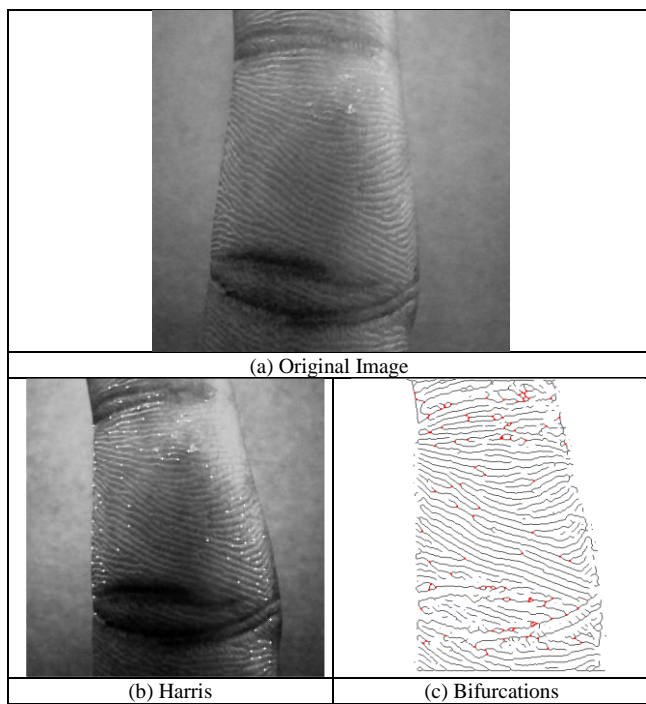

(a) Original Image

(b) Harris   (c) Bifurcations
Figure 4 : Example of landmarks detection

C. The Zernike moments

In (ρ, θ) polar coordinates, the Zernike radial polynomials of order p with repetition q are defined by[11]:

$$R_{pq}(\rho) = \sum_{s=0}^{\frac{p-|q|}{2}} \frac{(-1)^s (p-s)!}{s!\left(\frac{p+|q|}{2}-s\right)!\left(\frac{p-|q|}{2}-s\right)!} \rho^{p-2s} \qquad (3)$$

In the above equation p is a non-negative integer, (p$\geq$0), and q positive and negative integers subject to the constraints:

$$\begin{cases} p - |q| \ is \ even \\ \quad |q| \leq p \end{cases} \qquad (4)$$

The Zernike moment of order p with repetition q for a continuous image function $f(x,y)$, that vanishes outside the unit disk is:

$$Z_{pq} = \frac{p+1}{\pi} \iint_{x^2+y^2 \leq 1} V_{pq}^*(\rho,\theta) f(x,y)\, dx\, dy \qquad (5)$$

If F is the digital image of f , the above equation becomes [12]

$$Z_{pq} = \frac{p+1}{\pi} \sum_{x=1}^{N} \sum_{y=1}^{N} V_{pq}^*(\rho,\theta) F(x,y) \qquad (6)$$

with

$$V_{pq}(\rho,\theta) = R_{pq}(\rho) e^{iq\theta} \qquad (7)$$

where V_{pq}^* denote complex conjugate of V_{pq},
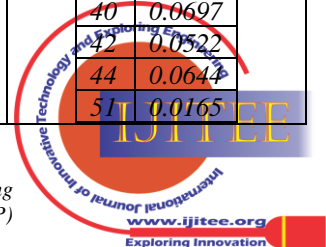$\rho = \sqrt{x^2+y^2} \leq 1$ et $\theta = tan^{-1}\left(\frac{y}{x}\right)$.

A study has shown that Zernike moments are less sensitive to noise and less redundant information [13]. Many other works like [11,14] were then performed on the invariance of the moments considering the affine transformation coordinates and intensity changes in grayscale images.

The defined features of Zernike moments themselves are only invariant to rotation. To obtain scale and translation invariance, the image needs to be normalized first by using the regular Zernike moments. Zernike features invariant to translation are then extracted from the normalized image [15].

Figure 5.1 shows an image, its corresponding 8° rotated and their Zernike moments. For the two images (see Figure 6), we have very close Zernike moments values.

Figure 5.2 shows another image and its corresponding 8° rotated and their Zernike moments. For the two images (see Figure 7), we have very close Zernike moment values. These values are all closer than their corresponding obtained from non skeletonized images (Figure 5.1).

(a) Image1		(b) Image1 rotated 8°	
pq	$|Z_{pq}|$	pq	$|Z_{pq}|$
00	0.2214	00	0.2406
11	0.0416	11	0.0432
20	0.1391	20	0.1474
22	0.1012	22	0.1123
31	0.0152	31	0.0207
33	0.0243	33	0.0253
40	0.0583	40	0.0697
42	0.0493	42	0.0522
44	0.0558	44	0.0644
51	0.0113	51	0.0165

53	0.0041		53	0.0069	
55	0.0033		55	0.0025	

1. Grayscale Images		

Skeleton of (a)	Skeleton of (b)

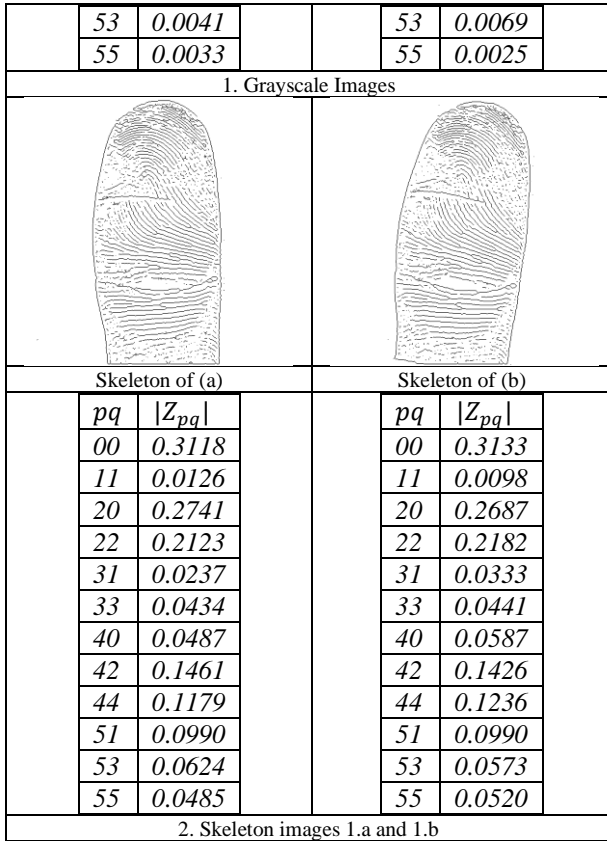| pq	$|Z_{pq}|$		pq	$|Z_{pq}|$	
00	0.3118		00	0.3133	
11	0.0126		11	0.0098	
20	0.2741		20	0.2687	
22	0.2123		22	0.2182	
31	0.0237		31	0.0333	
33	0.0434		33	0.0441	
40	0.0487		40	0.0587	
42	0.1461		42	0.1426	
44	0.1179		44	0.1236	
51	0.0990		51	0.0990	
53	0.0624		53	0.0573	
55	0.0485		55	0.0520	

2. Skeleton images 1.a and 1.b		

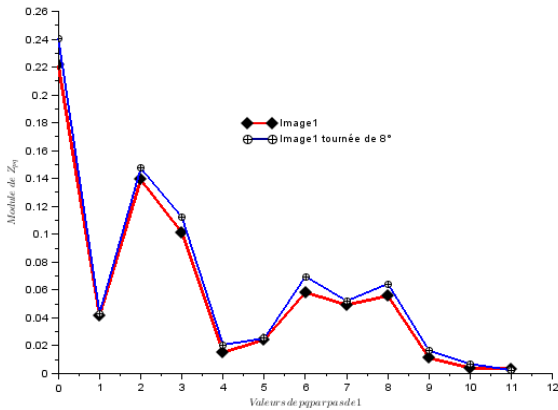Figure 5: Four fingerprint images and their Zernike moments

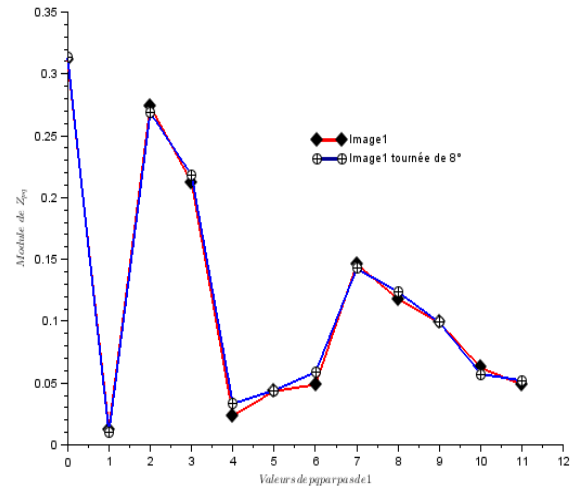Figure 6: Graphical Representation of the module of Zernike moments images (a) and (b) Figure 4.1

Figure 7: Graphical Representation of the module of Zernike moment of the skeleton images (a) and (b) Figure 5.2

D. Matching process

After extraction of landmark points of the images to readjust, we are left with two sets of points to match : a set of points on the reference image F_t and a set of points on the input image F_{t+d}. The correspondence between these two sets of control points is obtained by following steps:

■ Subdivide each image into thumbnail size RxR centered on each point P_i.

■ For each thumbnail centered on this point P_i, construct the descriptor vector of Zernike moments M_z as follows:

$$M_z = (|z_{11}|, \dots, |z_{pq}|, \dots, |z_{55}|) \tag{8}$$

where $|z_{pq}|$ is the module of Zernike moments. We have used as the highest order of moments 5 after several experimental trials. Although the higher order moments are the fine details of the image, they are more sensitive to noise than lower order moments

■ For any point r_i of the reference image, we suppose that its corresponding e_i of input image is from a set of points F_{t+d} located within a certain radius R_0 around r_i. The radius R_0 limits the search for corresponding and therefore, dramatically reduces the number of comparisons to achieve in order to find out the corresponding points.
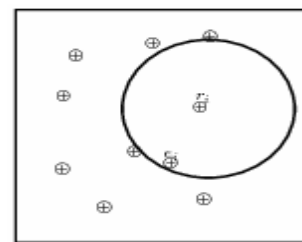
Figure 8: Determining the corresponding e_i (of input image F_{t+d}) of a point r_i (of the reference image F_t)

■ The matching process is performed by computing the correlation coefficients between the two descriptor vectors. The corresponding points are those which give the maximum value of correlation coefficients. The correlation coefficient between two vectors of the features $X(x_1, \ldots, x_n)$ and $Y(y_1, \ldots, y_n)$ is given by the following formula:

$$C = \frac{\sum_{i=1}^{n}(x_i - \bar{x})(y_i - \bar{y})}{\sqrt{\sum_{i=1}^{n}(x_i - \bar{x})^2} \times \sqrt{\sum_{i=1}^{n}(y_i - \bar{y})^2}} \qquad (9)$$

E. Deformation model

Once the information type to be used to guide the registration and the similarity criterion quantifying the similarity between two images are defined, the model of deformation is determined to realign the images. The geometric transformations or deformation models involved in the registration of 2D images are generally of rigid, affine or curvilinear [16].

The transformation model used to produce the image distortion F_{t+d} is the rigid transformation model expressed by Equation (10). Only rotation and translation are taken into account.

$$\begin{pmatrix} x' - x_0 \\ y' - y_0 \end{pmatrix} = \begin{pmatrix} cos\theta & -sin\theta \\ sin\theta & cos\theta \end{pmatrix}\begin{pmatrix} x - x_0 \\ y - y_0 \end{pmatrix} + \begin{pmatrix} t_x \\ t_y \end{pmatrix} \qquad (10)$$

where $M_0\begin{pmatrix} x_0 \\ y_0 \end{pmatrix}$ is the center of rotation, θ the angle of rotation, $\begin{pmatrix} t_x \\ t_y \end{pmatrix}$ the coordinates of the translation vector and $M'\begin{pmatrix} x' \\ y' \end{pmatrix}$, the transform of M.

The estimation of the parameters of the rigid transformation is carried out iteratively. At each iteration we provide online processing parameters found by RANSAC. The RANdom SAmple Consensus (RANSAC) is an algorithm proposed in 1981 by Fischler and Bolles[17]. It is a general parameter estimation approach designed to cope with a large proportion of outliers in the input data. This is a popular method in regression problems containing aberrant data or outliers[18].

IV. COMPARATIVE STUDY OF EXPERIMENTAL RESULTS

This section is dedicated to the comparative study of the performance of the two algorithms in terms of precision. In order to evaluate the precision of the registration algorithms, we have used a synthetic geometric distortion. The deformation model chosen was applied to a database of fingerprint images that we have formed. Our test image database consists of 100 grayscale images. Eight of them are shown in Figure 10.
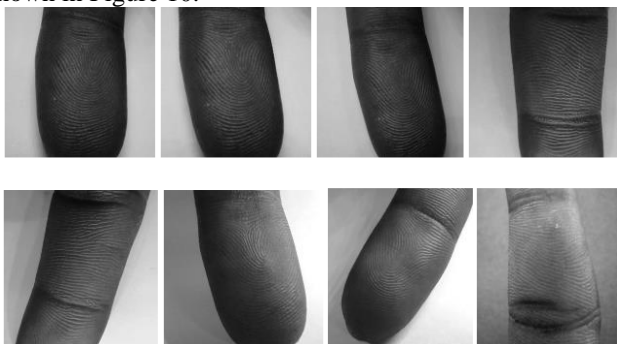

Figure 10: 8 images of 100 images contained in our database

The two algorithms have been implemented using Java. The test can be described by the following steps:

■ The Rotation and Translation transformations are applied to our images.

■ The error between the actual settings and those estimates is evaluated using the following equation:

$$\varepsilon_i = \frac{|\theta_i - \theta_i'|}{|\theta_i|} \qquad (11)$$

where ε_i is the error associated with estimating angles of the image i.

A. Relative error and execution time

As shown in table 1, the detection of points of interest based on bifurcation is more efficient in terms of reduced calculation time.

Method	Time (secondes)
Harris	0.428
Bifurcations	0.013

Table 1 – Execution time

The curve of errors referred to Figure 11. Table 2 shows a set of parameters characterizing the two methods. The maximum error was obtained by the Harris detector (see table 2 and Figure 11). This error is almost double that achieved by bifurcations. The mean of the error is 0.0162 for Harris and 0.0156 to the bifurcations.

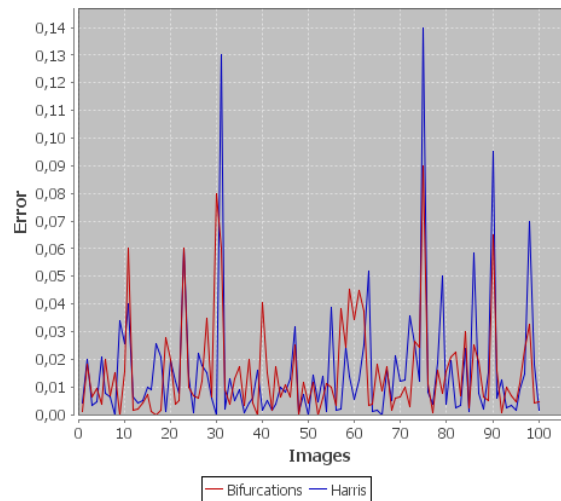| Method	Mean error	Min error	Max error	Variance
Bifurcations(M_1)	$x_1 = 0.01567437$	0.0	0.09	0.00030804
Harris (M_2)	$x_2 = 0.01632751$	0.0	0.14	0.00055208

Table 2 – Statistic parameter

Figure 11 – relative error curves

B. Statistics comparison of the algorithms

To compare the two methods, we use the statistical test of Student-Fisher[19,20]. This test takes place in two stages: one test in a first time equality of variances using the Fisher-Snedecor [21] test. In a second step, we test the equality of means with the result of the hypothesis of equality of variances.

1) Variances comparison

For this test, it makes hypothesis H_0 *and* H_1 following:

$$\begin{cases} H_0 \; : \; \sigma_1^2 = \; \sigma_2^2 \\ \\ H_1 \; : \; \sigma_1^2 > \; \sigma_2^2 \end{cases} \tag{12}$$

We compute the following statistics:

$$f_{obs} = \frac{\dfrac{n_1 \times S_1^2}{n_1 - 1}}{\dfrac{n_2 \times S_2^2}{n_2 - 1}} \tag{13}$$

S_1^2 *and* S_2^2 being respectively the variances from M_1 and M_2, $n_1 = n_2 = 100.$ We obtained $f_{obs} = 0.5579636.$
$P(F < f_{obs}) = 0.002018$ and the critical value of F is 0.7173286.

The p-value is less than 5%, we rejected the hypothesis that both methods have the same variance to the 5% threshold. This leads us to the next step.

2) Means comparison

Here we wish to test if M_1 is better than M_2 or not. We formulated null hypothesis «M_1 is no better than M_2» and the alternative hypothesis. «M_1 is better than M_2». Either $H_0 : m_1 = m_2$ against $H_1 : m_1 < m_2$. So it is in the presence of a one-sided test. Statistics t_{obs} related to this test is given by:

$$\boldsymbol{t_{obs}} = \frac{\overline{\boldsymbol{x_1}} - \overline{\boldsymbol{x_2}}}{\sqrt{\dfrac{\boldsymbol{S_1^2}}{\boldsymbol{n_1}} + \dfrac{\boldsymbol{S_2^2}}{\boldsymbol{n_2}}}} \tag{14}$$

We are $\boldsymbol{t_{obs}} = -0.2227$. $P(T < t_{obs}) = 0.412$ and the critical value of T is 1.653211. The critical value greater than the test statistic, we rejected null hypothesis in favor of his alternative to the 5% threshold. Thus M_1 is better than M_2.

In the light of the test, we can therefore say that the registration algorithm based on the ridge bifurcation gives better results compared to the method based on the Harris detector.

V. CONCLUSION

In this paper, we have discussed two contactless fingerprint images matching algorithms based on Zernike moment descriptors. The first algorithm uses classic minutiae (namely ridge bifurcation points) detector and the second algorithm uses Harris feature point detector. Despite the fact that Harris feature points are known to be easily matchable, our comparison have shown that the bifurcation points based algorithm perform better than the first one. In further works, we will pursue comparison with other feature points like fingerprint cores in contactless biometric systems.

REFERENCES

1. S. Pankanti, S. Prabhakar, A.K. Jain, On the individuality of fingerprints, IEEE Trans. Pattern Anal. Mach. Intell., 2002, 24 (8) 1010-1025.
2. Lifeng Liu, Tianzi Jiang, Jianwei Yang, and al. Fingerprint Registration by Maximization of Mutual Information, IEEE Transactions on image processing, May 2006, Vol. 15, No. 5, pp. 1100-1110.
3. C. Serief, Robust feature points extraction for image registration based on the nonsubsampled contourlet transform., International Journal Electronics Communication. 63 (2) (2009) 148-152.
4. Parziale, G., Santana, E-D., Hauke, R. The Surround Imager : A Multi-camera Touchless Device to acquire 3D Rolled-Equivalent Fingerprints. ICB2006, LNCS 3832, 2006, pp. 244-250.
5. B. Hiew, A. Teoh, and Y. Pang, Touch-less fingerprint recognition system, june 2007, pp. 24-29.
6. S. Mil'shtein, J. Palma, C. Liessner, M. Baier, A. Pillai, and A. Shendye, Line scanner for biometric applications, may 2008, pp. 205-208.
7. T. Djara, M. K. Assogba, A. Nait Ali. Caractérisation spatiale des empreintes de l'index en analyse biométrique. Actes du CARI 2010. Yamoussoukro. pp :501-508.
8. C. Harris and M. Stephens. "A combined corner and edge detector," in Proceedings of the 4th Alvey Vision Conference, pp. 147-151, 1988
9. H. Moravec. "Rover visual obstacle avoidance," in Proceedings of the 7th International Joint Conference on Artificial Intelligence, pp. 785-790, 1981.
10. H. Moravec. "Visual mapping by a robot rover," in Proceedings of the 6th International Joint Conference on Artificial Intelligence, pp. 598-600,1979.
11. R. J. Prokop and A. P. Reeves, A survey of moment-based techniques for unoccluded object representation and recognition, Computer Vision, Graphics, and Image Processing. Graphical Models and Image Processing, September 1992, vol. 54, No. 5, pp. 438-460.
12. R. Mukundan and K. R. Ramakrishnan, Moment Functions in Images Analysis. Theory and Applications, World Scientific, September 1998, 164pp.
13. W. Y. Kim and P. Yuan, A practical pattern recognition system for translation, scale, and rotation invariance, in Proceedings of the Conference on Computer Vision and Pattern Recognition, pages 391-396, Los Alamitos, CA, Etats-Unis. IEEE Computer Society Press, 1994
14. L. Van Gool and T. Moons and D. Ungureanu, Affine/photometric invariants for planar intensity patterns, in Proceedings of the 4th European Conference on Computer Vision, 1996, pp. 642-651.
15. A. Khotanzad and Y. H. Hong, Invariant image recognition by Zernike moments, IEEE Trans. Pattern Anal. Mach. Intell., May 1990, vol. 12, No. 5, pp.489-497.
16. P. A. ELSEN, E. J. D. POL and M. A. VIERGEVER, Medical image matching a review with classification, IEEE engineering in medecine and biology,march 1993, pp26-39.
17. M. A. Fischler and R. C. Bolles. Random Sample Consensus : A paradigm for model fitting with applications to image analysis and automated cartography. Communications of the ACM, June 1981, 24(6) :381-395.
18. Sunglok Choi, Taemin Kim and Wonpil Yu, Performance Evaluation of RANSAC Family. BMVC 2009 doi :10.5244/C.23.81
19. http://spiral.univ-lyon1.fr/mathsv/cours/stats/chap7/c7p4/c7p4.html
20. http://www.cmi.univ-mrs.fr/~kowalski/downloads/Enseignement/2008_2009/MASS/MSHE02/pdf/chapitre2.pdf
21. http://stat.ethz.ch/R-manual/R-patched/library/stats/html/var.test.html